

## The Influence of O<sub>2</sub> on the Corrosion Behavior of the X80 Steel in CO<sub>2</sub> Environment

Xiao Wang<sup>1</sup>, Xinyue Wang<sup>1</sup>, Jun Wang<sup>1,\*</sup>, Guowei Wang<sup>2</sup>, Yi Pan<sup>1</sup>, Shuangchun Yan<sup>1</sup>

<sup>1</sup> Liaoning Shihua University, Fushun, China;

<sup>2</sup> Northeast Petroleum of Pipeline Co.1st, Shenyang, China

\*E-mail: [mikewangjun@163.com](mailto:mikewangjun@163.com)

Received: 28 September 2019 / Accepted: 7 November 2019 / Published: 30 November 2019

---

The present paper investigates the influence of O<sub>2</sub> on X80 steel under the CO<sub>2</sub> environment through polarization curves, EIS, and employing characterization by corrosion images and mechanisms, using the test data of the environmental content of CO<sub>2</sub> and O<sub>2</sub> in an oil field, while the pressure of O<sub>2</sub> is 0.082bar~0.15bar. The results show that O<sub>2</sub> mainly have influence on the polarization process of X80 steel cathode, and in the low O<sub>2</sub> pressure of 0~0.12bar, corrosion potential and corrosion current density of X80 steel essentially remains the same, and with the increase of O<sub>2</sub> pressure to 0.17bar~0.22bar, comprehensive corrosion rate and the electric double layer capacitance all increase, and also the polarization resistance, diffusion resistance, and charge transfer resistance is reduced. This behavior can be attributed due to the fact that O<sub>2</sub> destroyed the surface of X80 steel by the corrosion film resulting in local corrosion caused by the presence of CO<sub>2</sub>.

---

**Keywords:** X80 steel; Carbon dioxide; Oxygen; Corrosion behavior; Film damage mechanism

### 1. INTRODUCTION

Nowadays, CO<sub>2</sub> flooding is an efficient and cost-efficient oil recovery method in producing oil reservoirs. However, it should be noted that this method can also lead to severe corrosion, resulting from a large amount of CO<sub>2</sub> in the produced water, where the H<sup>+</sup> is generated by ionization of H<sub>2</sub>CO<sub>3</sub> [1]. Moreover, the CO<sub>3</sub><sup>2-</sup> ionized from H<sub>2</sub>CO<sub>3</sub>, combined with calcium and magnesium ions, may promote the formation of scaling and depositing it on the inner wall of the pipe, which can provide conditions for SRB (Sulfate Reducing Bacteria) to accelerate corrosion under the scaling [2]. Related studies have shown that CO<sub>2</sub> has become the main factor for the corrosion of pipelines. In recent years, the economic losses due to the failure caused by the perforation of the pipes produced by the corrosion of CO<sub>2</sub> are increasingly prominent, rising to 6% of oil profits. Consequently, the corrosion caused CO<sub>2</sub> has attracted

extensive attention, and the investigations on the corrosion mechanism of pipelines became a research hotspot [3].

Compared with corrosion in the presence of pure CO<sub>2</sub>, the (co-)existence of O<sub>2</sub> may cause the activation and re-corrosion of the metal surface, and even induce further pitting and stress corrosion. Therefore, in the present paper, electrochemical investigations focusing on corrosion morphology, polarization curves and electrochemical impedance spectra (EIS) were carried out to explore the corrosion behavior of X80 steel in presence of NaCl solution containing O<sub>2</sub> and CO<sub>2</sub>, aiming to present the corrosion mechanism of O<sub>2</sub> on the corrosion performance of the X80 steel in CO<sub>2</sub> environment.

## 2. EXPERIMENT

### 2.1 Preparation

The traditional three-electrode system was adopted in this experiment, where the working electrode was X80 steel (10×10×2mm<sup>3</sup>), the reference electrode was SCE (saturated calomel electrode), and the auxiliary electrode was Pt. The reference electrode was in contact with the solution through the Luggin capillary, and the distance between its tip and the working electrode was less than 2mm to ignore the IR drop of the solution [4]. The working electrode was pretreated before the electrochemical test, as follows: (i) #800~1200 waterproof abrasive paper was applied to polish the electrode gradually to make the surface mirror-like, (ii) acetone and deionized water were used to clean the "working surface" of the electrode, and (iii) vacuum drying oven was applied in order to dry the sample.

Distilled water and analytically pure sodium chloride were used to prepare the experimental solution of the wt.3% NaCl solution.

### 2.2 Electrochemical test

Fig.1 shows the diagram of the electrochemical test for X80 steel in wt.3% NaCl solution with O<sub>2</sub>/CO<sub>2</sub>. All the tests were carried out in the reactor to control the temperature and pressure. The experimental temperature was set to 40°C, while the partial pressure of water vapor was 0.03 bar, in the case of CO<sub>2</sub> was 0.97 bar, while the partial pressure of O<sub>2</sub> (*p*-O<sub>2</sub>) was set to 0, 0.07 bar, 0.12 bar, 0.17 bar, and 0.22 bar, respectively. Once the open circuit potential (OCP) fluctuated less than 5mV within 300 s, the whole system was considered to be in a stable state [5]. At this time, the EIS and polarization curves were measured in sequence. The experiments were repeated twice to ensure the accuracy of the experiment.

The electrochemical working station was PARSTAT2273, and the results of the analysis were transferred to the "PowerSuite" and "ZSimpWin" software.

(1) Polarization curve test. The scanning rate of the polarization curve was set as 0.3mV/s, and the scanning potential range was ±250mV vs.OCP.

(2) EIS tests were performed for a range of 100kHz ~ 10mHz with an amplitude of 5mV.

### 2.3 Immersion experiment

Three pieces of X80 steel (size  $50 \times 25 \times 2 \text{ mm}^3$ ) were set simultaneously for the immersion experiment in the reactor. The pressures of  $\text{O}_2$  and  $\text{CO}_2$  in the reactor were kept unchanged during the time of the experimental, while the temperature was set to  $40^\circ\text{C}$ . After 7 days, the specimens were taken out to remove the corrosion products, and to investigate the corrosion morphology of the surface by SEM, and also, to calculate the average corrosion rate.

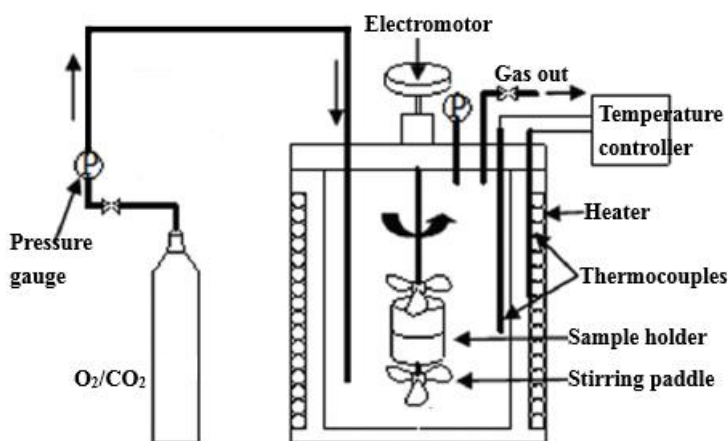


**Figure 1.** Electrochemical test for X80 steel in wt.3% NaCl solution with  $\text{O}_2/\text{CO}_2$

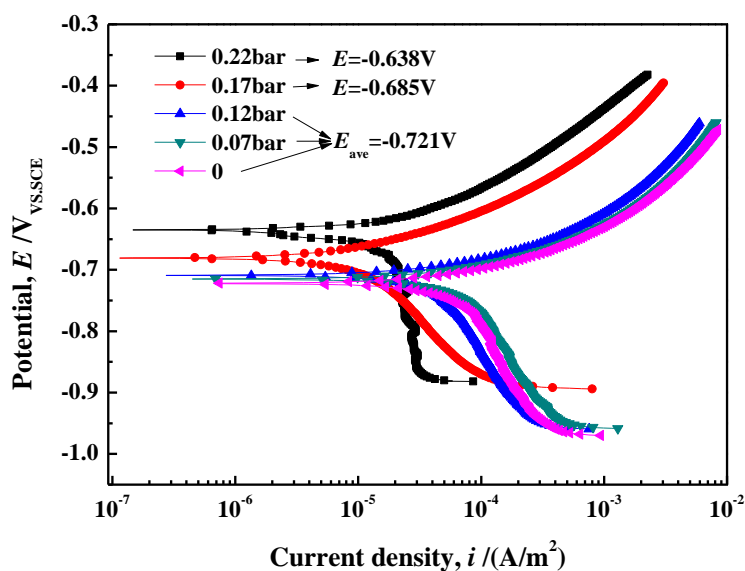
## 3. RESULTS AND DISCUSSION

### 3.1 Analysis of electrochemical test

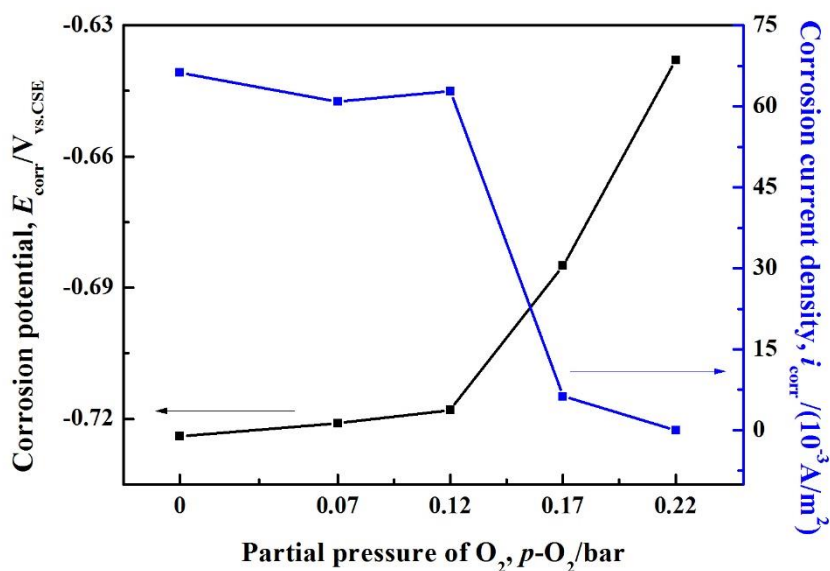
#### Polarization curve

Fig.2 shows the polarization curves of X80 steel under different  $p\text{-O}_2$  in  $\text{CO}_2$  environment, while the fitted results, including anodic- and cathodic- Tafel constant ( $b_a$  and  $b_c$ ), corrosion potential ( $E_{\text{corr}}$ ) and corrosion current density ( $i_{\text{corr}}$ ) are enlisted in Table 1. As can be seen from the Fig.2, when  $p\text{-O}_2$  gradually increased from 0 to 0.22bar, the  $b_c$  gradually decreased in parallel, meaning that  $\text{O}_2$  mainly affected the cathodic process on the surface of the steel. However, the anodic polarization curves kept unchanged with the same  $b_a$  as  $p\text{-O}_2$  rose up. Therefore, with the increasing  $p\text{-O}_2$ , the cathodic reaction process of X80 steel was changed from activated polarization control to diffusion control.

The other results were extracted from the  $E_{\text{corr}}$  and  $i_{\text{corr}}$ , at  $p\text{-O}_2=0\sim 0.12\text{bar}$ , where the  $E_{\text{corr}}$  (average= $-0.72\text{ V vs.SCE}$ ) and  $i_{\text{corr}}$  (average= $63.34 \times 10^{-3} \text{ A/m}^2$ ) changed a little, and there was no visible limit diffusion process in the cathodic region, suggesting that the low  $p\text{-O}_2$  had little influence on the cathodic process of X80 steel. Subsequently, as  $p\text{-O}_2$  continued to rise, the  $E_{\text{corr}}$  and  $i_{\text{corr}}$  dropped rapidly, at a  $p\text{-O}_2=0.22\text{ bar}$ , there was a visible region in cathodic curve caused by diffusion control of  $\text{O}_2$ , which may lead to induced pitting corrosion resulted by the damage of  $\text{CO}_2$  corrosion product film caused by  $\text{O}_2$  [6].



(1) Polarization curves of X80 steel



(2) Changes of  $E_{corr}$  and  $i_{corr}$  of X80 steel

**Figure 2.** Test results of polarization curves of the X80 steel under different  $p-O_2$  in a  $CO_2$  environment

**Table 1.** Fitted results of polarization curves of X80 steel under different  $p-O_2$  in  $CO_2$  environment

$p-O_2$ (bar)	$E_{corr}$ (V <sub>vs.CSE</sub> )	$b_a$ (mV)	$b_c$ (mV)	$i_{corr}$ ( $10^{-3}A/m^2$ )
0	-0.724	68	2350	66.27
0.07	-0.721	61	2241	60.92
0.12	-0.718	59	2300	62.84
0.17	-0.685	73	1460	6.29
0.22	-0.638	68	705	0.02

Electrochemical impedance spectrum (EIS)

Fig.3 shows the EIS results of X80 steel under different  $p\text{-O}_2$  in a  $\text{CO}_2$  environment. It can be seen that under different conditions of  $p\text{-O}_2$ , there were two capacitive reactance arcs in all EIS curves, indicating two time constants, which are related to two diffusion processes: low-frequency capacitive reactance arc representing the charge transfer process, while high-frequency capacitive reactance arc giving information about the mass transfer process [7,8]. Therefore, the proposed equivalent circuit is composed of solution resistance ( $R_s$ ), capacitance for whole system ( $Q$ ), in which due to dispersion effect [9], phase constant Angle element ( $Q$ ) was selected to replace the pure capacitance ( $C$ ), polarization resistance ( $R_p$ ), Warburg impedance ( $Z_w$ ) [10], capacitance for electric double layer ( $C_{dl}$ ) and charge transfer resistance ( $R_{ct}$ ), namely  $R_s(Q(R_p Z_w(C_{dl} R_{ct})))$ .

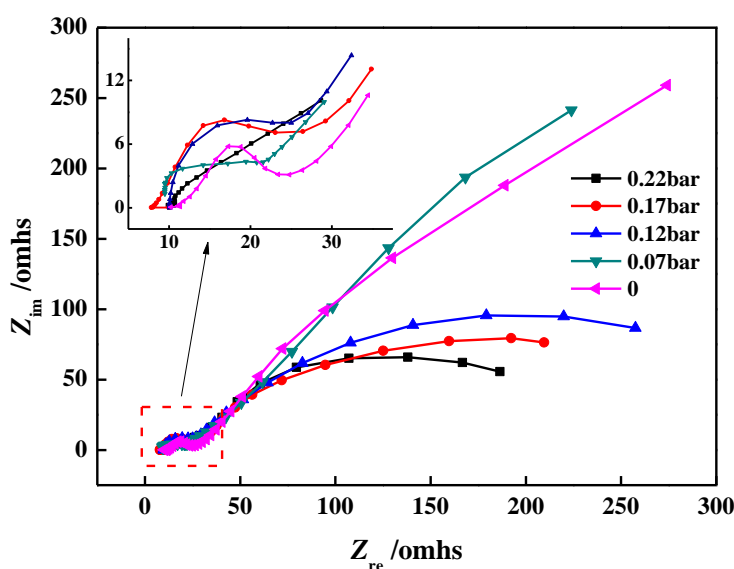
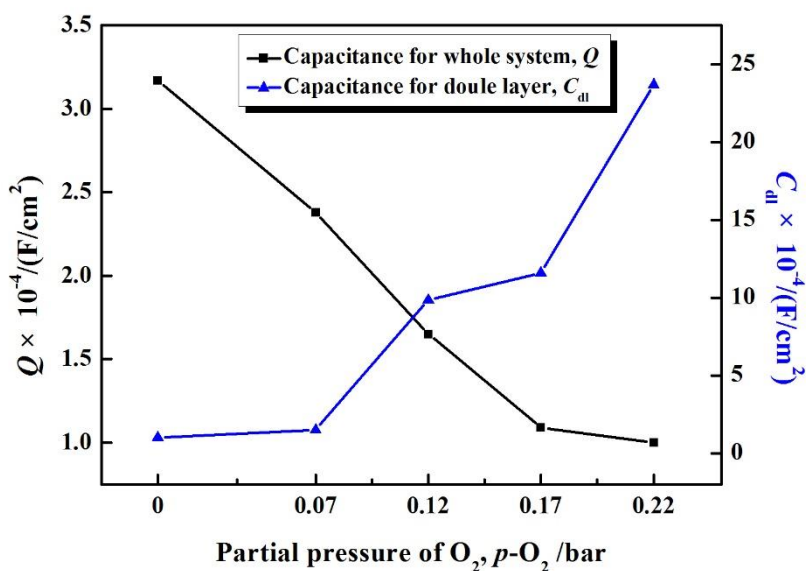


Figure 3. Test results of EIS of the X80 steel under different  $p\text{-O}_2$  in  $\text{CO}_2$  environment



(1) Changes of  $Q$  and  $C_{dl}$  of X80 steel

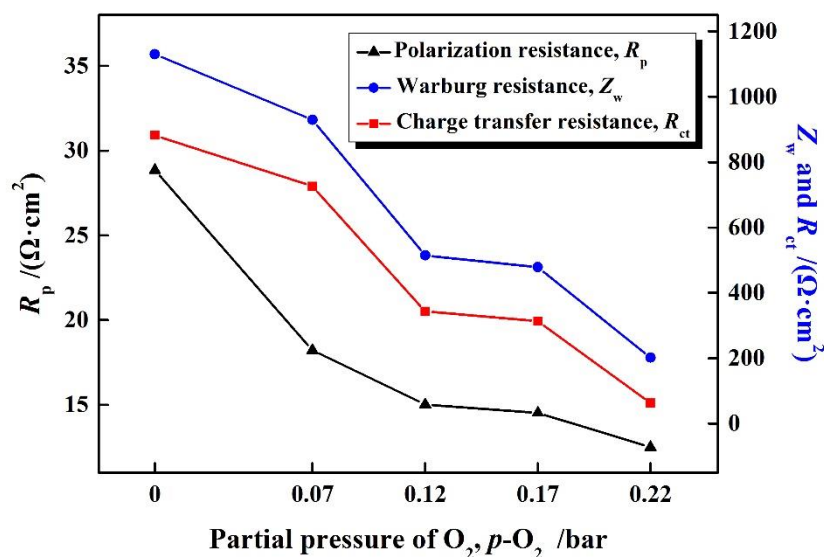
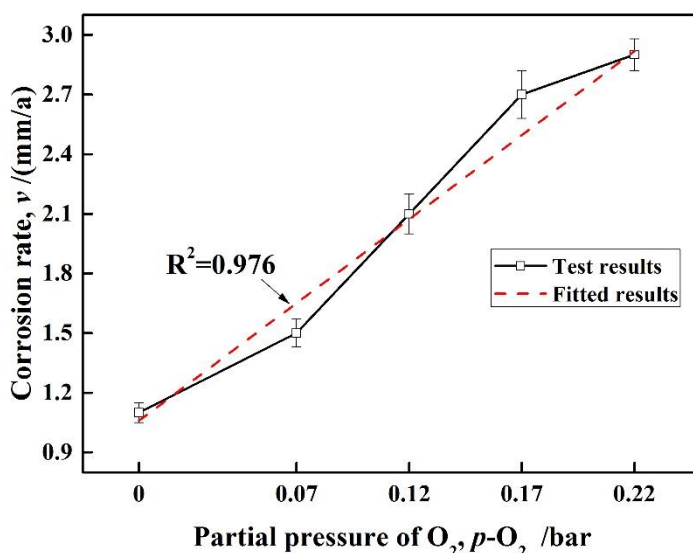
(2) Changes of  $R_p$ ,  $Z_w$  and  $R_{ct}$  of X80 steel**Figure 4.** Analyzed results of EIS of X80 steel under different  $p$ -O<sub>2</sub> in a CO<sub>2</sub> environment

Fig.4 shows the fitted results of EIS under different  $p$ -O<sub>2</sub> in a CO<sub>2</sub> environment. With the increase of  $p$ -O<sub>2</sub>, the capacitance for the whole system ( $Q$ ) decreased gradually, while capacitance for the electric double layer ( $C_{dl}$ ) increased. However, it was interesting that in parallel polarization resistance ( $R_p$ ), diffusion resistance ( $Z_w$ ) and charge transfer resistance ( $R_{ct}$ ) all decreased. This phenomenon can be attributed as follows: with the increase of  $p$ -O<sub>2</sub>, the dense product film formed on X80 steel in the CO<sub>2</sub> environment was damaged, making the loosed/porous corrosion products more likely to diffuse into the solution, so as  $Q$  and  $R_p$  gradually decreased. At the same time, due to the reduction of O<sub>2</sub>, the speed of the charge transfer was accelerated, proven by the increase of  $C_{dl}$  and the decrease of  $R_{ct}$ .

### 3.2 Analysis of immersion test

#### Corrosion rate

Fig.5 shows the average corrosion rate of X80 steel under different  $p$ -O<sub>2</sub> in a CO<sub>2</sub> environment. As can be seen, with the increase of  $p$ -O<sub>2</sub>, the average corrosion rate mostly showed a linear relationship with  $p$ -O<sub>2</sub>, suggesting that the  $p$ -O<sub>2</sub> increased from 0 to 0.22bar, only 23% of CO<sub>2</sub> pressure, however, the corrosion rate caused by O<sub>2</sub> increased 260%, which indicated that in the CO<sub>2</sub> environment, O<sub>2</sub> would accelerate the corrosion rate and became the main factor. This can be explained by the damage of the film produced in the CO<sub>2</sub> environment, caused by the presence of O<sub>2</sub>.



**Figure 5.** The corrosion rate of X80 steel under different *p*-O<sub>2</sub> in a CO<sub>2</sub> environment

### Corrosion morphology

Fig.6 shows the surface morphology of X80 steel corrosion products under different *p*-O<sub>2</sub> in a CO<sub>2</sub> environment. It can be seen that in the pure CO<sub>2</sub> environment, a dense corrosion product film was formed on the surface of the X80 steel after 7 days, which was mainly composed of prismatic FeCO<sub>3</sub>. In the corrosive environment with *p*-O<sub>2</sub>=0.22bar, only partial and incomplete corrosion products were produced, making the cover of the surface of X80 steel incomplete. The main reason for this phenomenon can be attributed to the presence of dense FeCO<sub>3</sub> film formed on the surface of the metal, while the further oxidation of FeCO<sub>3</sub> resulted in the damage of product film due to the presence of O<sub>2</sub> [11]. Therefore, in the present research, the X80 steel was first put into a pure CO<sub>2</sub> environment for 72h and then inserted into a 0.22 bar of O<sub>2</sub> for 96 h to confirm the changes of its corrosion morphology products, as it is shown in Fig.7.

After 48h, a dense FeCO<sub>3</sub> film was formed on the surface of X80 steel in a CO<sub>2</sub> environment. Once O<sub>2</sub> entered into the CO<sub>2</sub> environment (with *p*-O<sub>2</sub>=0.22 bar and for 96 h), there was a bulge on the surface of the electrode, caused by the damage of FeCO<sub>3</sub> film, in which corrosion fissures were forming to make more accentuated the corrosion medium absorption, in order to promote the corrosion reaction of the metal-matrix. At the same time, Fe<sup>2+</sup> via a microscopic channel on the defect was diffused into the solution, in which electric couple corrosion was occurred, inducing pitting corrosion or stress crack.

Moreover, in a pure CO<sub>2</sub> environment, uniform and complete corrosion product film were composed mostly of FeCO<sub>3</sub>, formed on the surface of the steel, preventing it from further corrosion. However, as *p*-O<sub>2</sub> increased, the occurrence of surface fissures destroyed the integrity of FeCO<sub>3</sub> film and promoted the corrosion crevice, absorbing more corrosion medium, (re)activating the reaction of metal-matrix again [12]. Moreover, electric couple corrosion was preferred to occur in these defects, inducing pitting corrosion or stress crack.

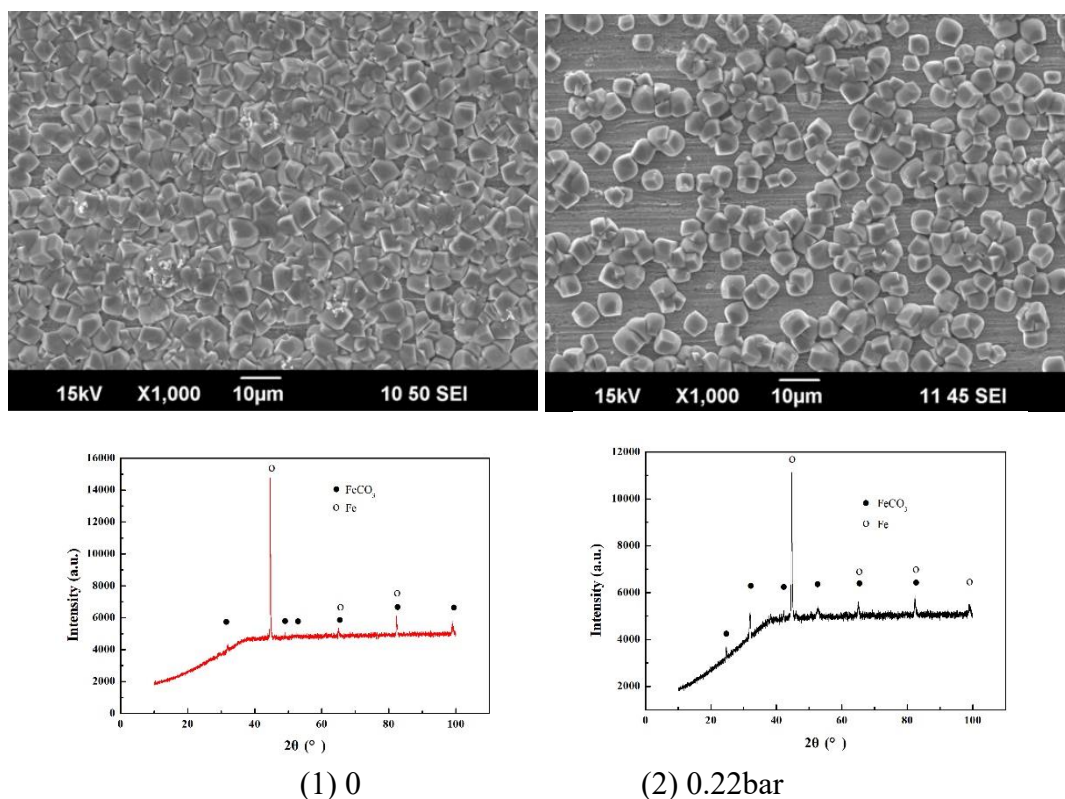


Figure 6. Corrosion morphology of X80 steel under different  $p\text{-O}_2$  in a  $\text{CO}_2$  environment

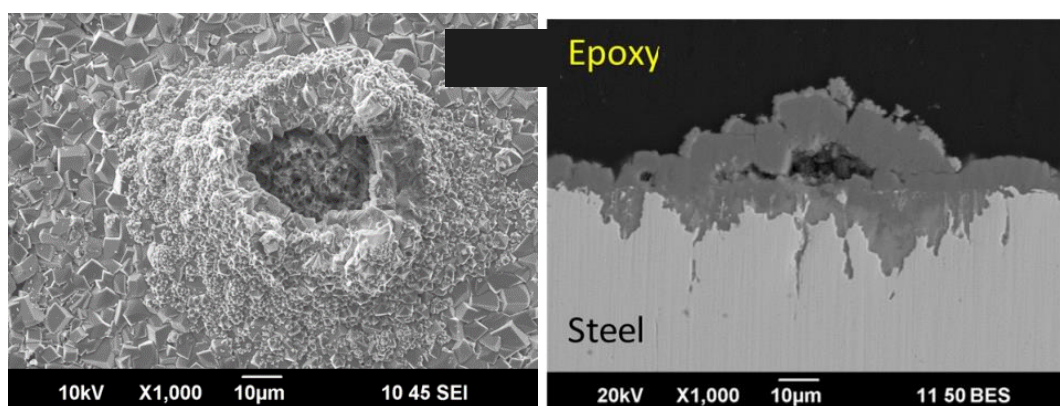
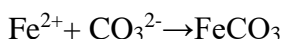
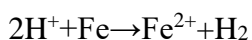


Figure 7. The morphology of  $\text{CO}_2$  corrosion product film in the presence of  $\text{O}_2$

### 3.3 Corrosion mechanism caused by $\text{O}_2/\text{CO}_2$

From the above-mentioned experimental results, it can be observed that the layer of corrosion product film formed on the surface of X80 steel in a  $\text{CO}_2$  environment has a good protective effect. However,  $\text{O}_2$  destroyed this  $\text{FeCO}_3$  film, resulting in the activation of the further corrosion reactions. The reaction process can be divided into five main stages.

(a) In a pure  $\text{CO}_2$  environment, dense  $\text{FeCO}_3$  film was formed on the surface of X80 steel to prevent further corrosion [13], as it can be seen in Fig.8(a), describable with the following equations:



(b)  $\text{FeCO}_3$  product with the reductive feature was gradually oxidized to  $\text{Fe}^{3+}$  once  $\text{O}_2$  diffused into the  $\text{CO}_2$  environment and furtherly generating porous  $\text{Fe}_2\text{O}_3$  [14] ( $4\text{FeCO}_3 + \text{O}_2 \rightarrow 2\text{Fe}_2\text{O}_3 + 4\text{CO}_2$ ), as shown in Fig.8(b);

(c) In the third stage,  $\text{O}_2$  gradually penetrated the  $\text{FeCO}_3$  film, furtherly destroying the dense  $\text{FeCO}_3$  layer on the surface of steel [15] (Fig.8(c));

(d) The acidification in inner  $\text{FeCO}_3$  film as  $\text{O}_2$  penetrated into the  $\text{FeCO}_3$  film, which may be caused by two aspects: (i) the ionization of  $\text{H}_2\text{CO}_3$ , and (ii) hydrolytic of  $\text{Fe}^{2+}$  ( $\text{Fe}^{2+} + \text{H}_2\text{O} \rightarrow \text{Fe}(\text{OH})_2 + 2\text{H}^+$ ), which all contributed to the pH reduction [16,17]. The acidification in the micro-pores promoted the dissolution of  $\text{FeCO}_3$  and then produced  $\text{CO}_2$ , while  $\text{H}^+ \rightarrow \text{H}_2$  was trapped in the micro-pores. As time advanced, the pressure in micro-pores rose up, leading to the formation of surface bulges [18], mentioned in the section of Corrosion morphology (Fig.8(d));

(e) The continuous consumption of  $\text{O}_2$  in corrosion crevice promoted the formation of oxygen concentration difference battery, in which the inner worked as anodic region, while the outer one was the cathodic region, aggravating the acidification of crevice. The lower pH also accelerated the dissolution of the metal-matrix, increasing, even more, the local corrosion. As the internal pressure continued to increase, the top of surface bulge broken, releasing the trapped  $\text{CO}_2$  and  $\text{H}_2$  into the solution (Fig.8(e)). Furthermore, the complete and dense  $\text{FeCO}_3$  film was gradually destroyed.

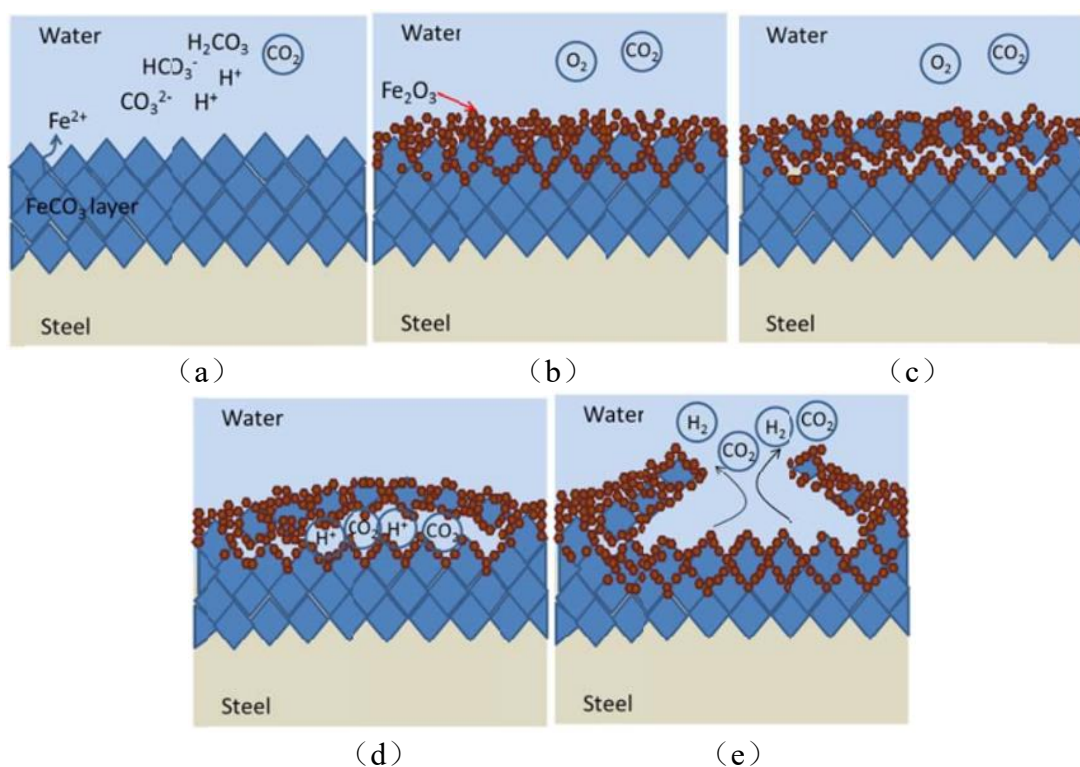


**Figure 8.** Mechanism of failure of  $\text{CO}_2$  corrosion product film by  $\text{O}_2$

#### 4. CONCLUSION

In the present paper, the corrosion mechanism of O<sub>2</sub> on the corrosion performance of the X80 steel in CO<sub>2</sub> environment was presented. The results can be discussed based on two main phenomena/cases:

(1) In CO<sub>2</sub> environment, O<sub>2</sub> mainly affects the cathodic polarization process of X80 steel in NaCl solution. At  $p\text{-O}_2=0\sim 0.12\text{bar}$ ,  $E_{\text{corr}}$  and  $i_{\text{corr}}$  of X80 steel all remain the same, and with the increase of  $p\text{-O}_2$ , the corrosion rate of X80 steel increases linearly, illustrating that  $E_{\text{corr}}$  moves positively and  $i_{\text{corr}}$  decreases, while  $Q$  and  $R_p$  gradually decreased. At the same time, due to the reduction of O<sub>2</sub>, the charge transfer speed was accelerated, proven by the increase of  $C_{\text{dl}}$  compared to the decrease of  $R_{\text{ct}}$ , which can be explained by the damage of CO<sub>2</sub> corrosion product film caused by O<sub>2</sub>, inducing localized corrosion.

(2) The film damage mechanism can explain the corrosion mechanism of O<sub>2</sub> on X80 steel in CO<sub>2</sub> environment. While in pure CO<sub>2</sub> environment, the whole surface of X80 steel is covered with FeCO<sub>3</sub>, as O<sub>2</sub> diffuses into the CO<sub>2</sub> environment, the corrosion products are transformed into loose and porous Fe<sub>2</sub>O<sub>3</sub>. The penetration of O<sub>2</sub> into FeCO<sub>3</sub> film promotes the solubility of FeCO<sub>3</sub> and acidification of the crevice, accelerating the generation of CO<sub>2</sub> and H<sub>2</sub>. As time goes on, the inner pressure damages the surface bulge, releasing CO<sub>2</sub> and H<sub>2</sub> into solution.

#### References

1. G.A. Zhang and Y.F. Cheng, *Electrochim. Acta*, 56 (2011) 1676.
2. D. Xu, W. Huang, G. Ruschau, J. Hornemann, J. Wen, and T. Gu, *Eng. Fail. Anal.*, 28 (2013) 149.
3. S. Nestic, *Corros. Sci.*, 49 (2007) 4308.
4. L.V.S. Philippe, S.B. Lyon, C. Sammon, and J. Yarwood, *Corros. Sci.*, 50 (2008) 887.
5. L.Y. Xu, X. Su, Z.X. Yin, Y.H. Tang, and Y.F. Cheng, *Corros. Sci.*, 61 (2012) 215.
6. J. Niteen and G.V. Johnston, *J. Electrochem. Soc.*, 116 (2019) C3461.
7. L. Caeres, T. Vargas and L. Herrera, *Corros. Sci.*, 51 (2009) 971.
8. L. Caeres, T. Vargas and M. Parra, *Electrochim. Acta*, 54 (2009) 7435.
9. S.M. Hoseinie, A.M. Homborg, T. Shahrabi, J.M.C. Mol and B. Ramezanzadeh, *Electrochim. Acta*, 217 (2016) 226.
10. B. Hirschorn, M.E. Orazem, B. Tribollet, V. Vivier, I. Frateur and M. Musiani, *Electrochim. Acta*, 55 (2010) 6218.
11. Ph. Refait, M. Jeannin, R. Sabot, H. Antony and S. Pineau, *Corros. Sci.*, 90 (2015) 375.
12. A. Ejaz, Z.P. Lu, J.J. Chen, Q. Xiao, X.K. Ru, G.D. Han and T. Shoji, *Corros. Sci.*, 10 (2015) 165.
13. Y. Hua, S.S. Xu, Y. Wang, W. Taleb, J.B. Sun, L. Zhang, R. Barker and A. Neville, *Corros. Sci.*, 157 (2019) 392.
14. D.Y. Wang, Z.W. Zhu, N.F. Wang, D. Zhu and H.R. Wang, *Electrochim. Acta*, 156 (2015) 301.
15. W.H. Wang, K.L. Shen, S. Tang, R.Q. Shen, T. Parker and Q.S. Wang, *Process Saf. Environ.*, 130 (2019) 57.
16. G. Tranchida, M. Clesi, F. Di Franco and M. Santamaria, *Electrochim. Acta*, 273 (2018) 412.
17. S.P. Sah, E. Tada and A. Nishikata, *Corros. Sci.*, 133 (2018) 310.
18. X.Q. Lin, W. Liu, F. Wu, C.C. Xu, J.J. Dou and M.X. Lu, *Appl. Surf. Sci.*, 329 (2015) 104.